Pure Appl. Geophys. 176 (2019), 4415–4430

https://doi.org/10.1007/s00024-019-02185-5

Pure and Applied Geophysics

Investigating the Contribution of Stress Drop to Ground-Motion Variability by Simulations Using the Stochastic Empirical Green's Function Method

Hongwei Wang,[1,2] Yefei Ren,[1,2] Ruizhi Wen,[1,2] and Peibin Xu[1,2]

Abstract—The stress drop ($\Delta\sigma$) is a fundamental parameter used to quantify source physics, and its uncertainty is closely related to seismic hazard. To reveal the relationship between $\Delta\sigma$ uncertainty and resultant ground-motion variability, ground motions produced by the 2013 M_w6.6 Lushan earthquake, characterized by various $\Delta\sigma$ values, are simulated using the stochastic empirical Green's function method. First, the variability in spectral amplitudes of simulated ground motions arising from the stochastic rupture process is investigated. Generally, it increases from $\sim$ 0.05 to $\sim$ 0.14 as the period increases up to 2.0 s, irrespective of the $\Delta\sigma$ value used. The ground-motion variability due to $\Delta\sigma$ uncertainty is then explored. The synthetic spectral amplitude is found to be linearly proportional to $\Delta\sigma^b$, thus the standard deviation of $\Delta\sigma$ (log10 unit) is equal to the standard deviation of the spectral amplitude (log10 unit) multiplied by a factor b. The regressed b values are strongly dependent on the period and generally in the range of 0.7 to 0.6 up to the period of 2.0 s. These results explain how much of the ground-motion variability is caused purely by $\Delta\sigma$ uncertainty. Moreover, the standard deviation of the spectral amplitudes is calculated directly from simulations based on random $\Delta\sigma$ values following a lognormal distribution. The findings further verify the reliability of the relationship between $\Delta\sigma$ uncertainty and ground-motion variability. Assuming that the interevent standard deviation in a ground-motion prediction model is dominated entirely by $\Delta\sigma$ uncertainty and the stochastic rupture process, we estimate the standard deviation of $\log_{10}\Delta\sigma$ ($\sim$ 0.2–0.3) for broad regions using various models.

Key words: Ground motion, stress drop, variability, simulation, Lushan earthquake.

1. Introduction

The stress drop ($\Delta\sigma$) is one of the key parameters in earthquake source physics because it is related directly to the high-frequency region of the source spectrum (Brune 1970). It is commonly calculated from the corner frequency (f_c) and the seismic moment (M_0), measured from observed ground motions by means of various approaches (e.g., Allmann and Shearer 2009; Baltay et al. 2011; Oth et al. 2017), in accordance with a circular crack model (Brune 1970; Eshelby 1957; Madariaga 1976). Many previous studies have confirmed that stress drops estimated by M_0–f_c analysis show exceptionally large scatter with variations on the order of $\sim 10^3$ or more (e.g., Allmann and Shearer 2009; Cocco et al. 2016; Courboulex et al. 2016; Oth et al. 2017). Statistically, it has been established that stress drops follow a lognormal distribution with mean of $\sim$ 3 and $\sim$ 6 MPa for inter- and intraplate earthquakes, respectively (Allmann and Shearer 2009).

Recently, many studies have been performed to interpret the large scatter in stress drops estimated by M_0–f_c analysis based on observed ground motions; For example, Cotton et al. (2013) found that error propagated from corner frequency estimation led to expansion of the variability in estimated stress drops, which was, on average, roughly 3–4 times larger than expected based on the interevent standard deviation (τ) of peak ground acceleration (PGA) reported by ground-motion prediction equations (GMPEs). Abercrombie (2015) systematically investigated the uncertainties of stress drops calculated using a method based on the empirical Green's function (EGF), i.e., ground-motion recording from a smaller earthquake. They found that uncertainties decrease as

[1] Institute of Engineering Mechanics, China Earthquake Administration, No. 29 Xuefu Road, Harbin 150080, People's Republic of China. E-mail: ruizhi@iem.ac.cn

[2] Key Laboratory of Earthquake Engineering and Engineering Vibration, China Earthquake Administration, Harbin, People's Republic of China.

the number of stations and EGFs used is increased. In addition, the natural randomness of the source kinematic process (Causse et al. 2014), limitations of the standard assumption of a symmetrical circular source (Kaneko and Shearer 2014, 2015), inappropriate hypothesis of independence between rupture velocity and stress drop (Causse and Song 2015), and application of mixed ground-motion data from different regions (Oth et al. 2017) have all been proposed to explain the large scatter in estimated stress drops. However, it remains to be clarified how much of the variability in the stress drop from observed ground motions is likely to be true source variability.

It is well known that stress drop persistently exerts inevitable effects on ground motion (Abrahamson et al. 2014; Baltay and Hanks 2014). Robust prediction of ground motion, especially that expected in future earthquakes, is dependent directly or indirectly on the stress drop determined, for example, by the stochastic method (Boore 2003) or by the EGF method (Irikura 1983). In general, the stress drop of a target earthquake (i.e., a future or historical earthquake for which ground motions need to be simulated) cannot actually be determined in advance because of the unavailability of measurements (Kanamori 1994). The stress drop has long been one of the fundamental elements of source physics considered in the evaluation of variability in simulated ground motions (e.g., Beauval et al. 2009; Bjerrum et al. 2013; Causse et al. 2008; Sørensen et al. 2007). However, quantification of the ground-motion variability resulting from the stress drop has not been considered in previous studies. This inspired us to explore the inherent relationship between stress drop variability and ground motion using simulations.

Different from the classical EGF method (Irikura 1983), the stochastic EGF method (Kohrs-Sansorny et al. 2005) assumes the target earthquake as a symmetrical circular source. In this method, the source rupture process of the target earthquake is represented by a series of subruptures corresponding to the rupture of the EGF event (i.e., a smaller earthquake for which EGFs were collected) that occurred at some point during the total source duration. The source rupture process is generated stochastically according to a specific probability density function in relation to the seismic moment and stress drop. The source of the target earthquake can thus be described by two parameters: stress drop and seismic moment. Stress drop remains the only variable in the simulation, because the seismic moment can be easily determined. This method affords the potential to investigate the variability of ground motion due to stress drop uncertainty. In previous studies (e.g., Courboulex et al. 2010; Honoré et al. 2011), this method was used to explain the notable influence of stress drop uncertainty on simulated spectral amplitudes.

In this study, the stochastic EGF method is used to simulate ground motions produced by the 2013 M_w6.6 Lushan earthquake in China, characterized by various stress drop values. First, the ground-motion variability arising from stochastic rupture processes is investigated. Then, we explore the potential relationship between ground motion and stress drop. Finally, we evaluate the ground-motion variability caused purely by stress drop uncertainty. Moreover, the ground-motion variability resulting from random stress drop values following a lognormal distribution in a series of collections with various standard deviations is computed directly to verify the reliability of the relationship between ground-motion variability and stress-drop variability.

2. *Stochastic EGF Method*

In the stochastic EGF method (Kohrs-Sansorny et al. 2005), simulated ground motion is expressed as the convolution between the EGF defining the path and site effects and an equivalent source time function (ESTF) representing the source rupture process, i.e., $S(t) = \mathrm{ESTF}(t) * EGF(t)$. The ESTF is generated stochastically in two steps. In the first step, a number η_c of time delays t_c is generated randomly following a probability density function $\rho_c(t)$ within the source duration T_c. In the second step, a number η_d of time delays t_d is generated randomly following another probability density function $\rho_d(t)$ within a window duration $T_d \leq T_c$, centered on each time delay generated in the first step. Finally, $\eta = \eta_c\eta_d$ small events are summed and scaled by a factor κ. Thus, the ESTF representing the i-th stochastic rupture process can be expressed as

$$\mathrm{ESTF}_i(t) = \kappa \sum_{d=1}^{\eta_d} \sum_{c=1}^{\eta_c} \delta[t - t_c(i) - t_d(i)], \quad (1)$$

where δ is the Dirac delta function.

Under two conditions, viz. (1) the scaling relation of the well-known omega-squared source spectra (Brune 1970), which is the exact agreement between the Fourier amplitude spectral ratio of the simulated ground motion averaged over all stochastic rupture processes to the EGF and the omega-squared source spectral ratio of the target earthquake to the EGF event, and (2) earthquake self-similarity (Kanamori and Anderson 1975), the fundamental parameters [η, κ, $\rho_c(t)$, and $\rho_d(t)$] can be determined to generate the ESTFs. η and κ can be expressed as

$$\eta = N^4, \quad \text{and} \quad \kappa = C/N, \quad (2)$$

where $N = f_{cS}/f_{cL}$, $C = \Delta\sigma_L/\Delta\sigma_S$, and

$$CN^3 = M_{0L}/M_{0S}. \quad (3)$$

The subscripts "L" and "S" in Eq. (3) indicate the target (larger) and EGF (smaller) events, respectively. The parameter C represents the ratio between the stress drop of the target event ($\Delta\sigma_L$) and that of the EGF event ($\Delta\sigma_S$). It mainly constrains the high-frequency spectral level of the simulated ground motion. Much greater high-frequency spectra and shorter durations would be expected in the simulated ground motions for a larger C value. In this study, the relation $\eta_c = \eta_d$ is considered. The probability density functions $\rho_c(t)$ and $\rho_d(t)$ are expressed as functions of the stress drop and seismic moment for both the target and EGF events in detail in Appendix A of Kohrs-Sansorny et al. (2005). Following Eshelby (1957) and Brune (1970), f_c can be expressed as

$$f_c = 0.37\beta\left(\frac{16}{7}\frac{\Delta\sigma}{M_0}\right)^{1/3}, \quad (4)$$

where β is the shear wave velocity, set to 3.6 km/s in this study. The source duration T_c is defined as $1/f_{cL}$. The window duration T_d can be expressed as $(f_{cS}f_{cL})^{-1/2}$, a constant value dependent on the corner frequencies of the target and EGF events.

3. Lushan Earthquake and Its Stress Drop Estimation

The Lushan earthquake occurred on 20 April 2013 on the southwestern segment of the SW–NE-trending thrust-slip Longmenshan fault belt, ~ 70 km southwest of the location of the 2008 Great Wenchuan earthquake. Its surface wave magnitude (M_s) was measured at 7.0 by the China Earthquake Network Center, and its moment magnitude (M_w) was measured at ~ 6.6–6.7 (Hao et al. 2013; Wang et al. 2013a; Zhang et al. 2014). In this study, the value of M_w = 6.6 is adopted. This earthquake was a shallow intraplate blind-thrust event with hypocentral depth of 13 km (measured by the China Earthquake Network Center). It has no rupture directivity according to the inverted kinematic rupture models (Hao et al. 2013; Wang et al. 2013a; Zhang et al. 2014). Most of the energy in this earthquake was released within the first 10 s following the initial rupture, and the slips were nucleated mainly in a narrow area approximately centered on the point of initial rupture. A moderate earthquake such as the Lushan event with no rupture directivity is particularly suitable for simulations by the stochastic EGF method.

In this study, an aftershock that occurred on 20 April 2013 at 01:02:58 (UTC), which was measured at M_s 4.9 by the China Earthquake Network Center, is selected as an EGF event of the Lushan earthquake. The two events have adjacent hypocentral locations and similar focal mechanisms, as reported by Lyu et al. (2013). The moment magnitude, corner frequency, and Brune-type stress drop of this EGF event are 4.57, 1.12 Hz, and 2.049 MPa, respectively, as estimated from the S-wave spectral inversion analysis by Wen et al. (2015). Strong-motion recordings obtained during the EGF event at 16 stations (Fig. 1), which recorded the Lushan earthquake simultaneously, were used as the EGFs. The strong-motion recordings were processed uniformly, including baseline correction and Butterworth bandpass filtering between 0.2 and 30.0 Hz.

The universally accepted method for the estimation of the stress drop, a vital parameter in blind ground-motion simulation, has remained ambiguous to date, although various strategies have been adopted (e.g., Pulido et al. 2004; Sharma et al. 2013; Wang

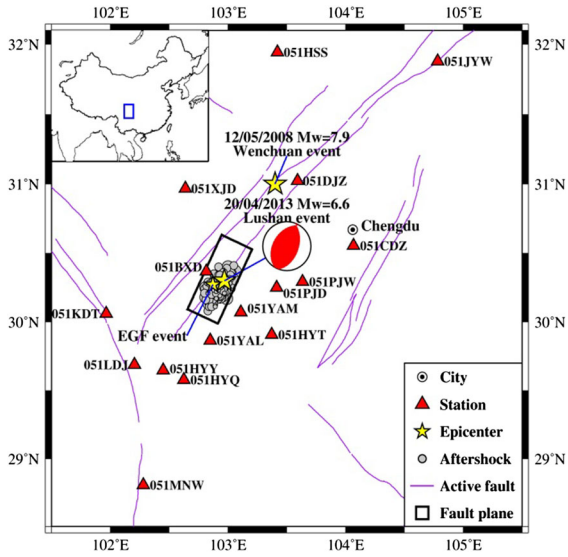

Figure 1
Locations of the Lushan earthquake and M_s 4.9 aftershock taken as the empirical Green's function (EGF) event (stars). Earthquakes in the Lushan seismic sequence are marked with solid gray circles. Recordings obtained at 16 stations (triangles) for the EGF event were regarded as EGFs for the ground-motion simulation. Active fault traces (solid lines) and epicenters (stars) of the 2008 Wenchuan earthquake are also plotted. The inset in the top-left corner indicates the region of study

et al. 2017; Zafarani et al. 2012). In some other studies (e.g., Courboulex et al. 2010; Honoré et al. 2011; Salichon et al. 2010), GMPEs have been taken as measures for calibrating the stress drop ratio between target and EGF events that could be considered optimum in a set of assumed values. In this study, multiple values of the stress drop of the Lushan earthquake were estimated in accordance with various current approaches, as described briefly in the following and listed in Table 1.

1. For a circular fault in an entire space, Eshelby (1957) expressed the average stress drop on a ruptured plane in relation to the seismic moment and rupture radius. The rupture radius can be obtained from the total rupture area estimated empirically based on the relationship between the total rupture area and the seismic moment. Stress drops were estimated at 2.31 and 3.60 MPa in accordance with the empirical relations proposed by Somerville et al. (1999) and Wells and Coppersmith (1994), respectively.
2. A dynamic model for rupture of a circular fault with an asperity at its center, which was proposed by Das and Kostrov (1986), was used by Pulido et al. (2004) to estimate the average stress drop on a rupture plane. They obtained an expression for the stress drop in relation to the seismic moment and the total rupture area based on an empirical ratio of 22% between the asperity area and the total rupture area (Somerville et al. 1999). The total rupture area can be estimated from its empirical relationship with the seismic moment. Stress drops of 4.13 and 6.425 MPa were derived using the empirical relationships proposed by Somerville et al. (1999) and Wells and Coppersmith (1994), respectively.
3. Dalguer et al. (2008) calibrated a set of dynamic rupture models using the stress-drop distribution on a fault and the average stress drop. They suggested that the average stress drop varies as the ratio of the rupture length to the maximal rupture width increases. Wang et al. (2017) used these dynamic models to retrieve an average stress drop of 1.5 MPa for the Lushan earthquake, consistent with the result provided by Hao et al. (2013) based on an inverted kinematic source model.
4. The average stress drop of many earthquakes was regarded as that of the target earthquake in the same tectonic environment by Zafarani et al. (2012). Wen et al. (2015) calculated Brune-type stress drops for 30 earthquakes of M_s = 3.5–5.4 in the Lushan seismic sequence. The derived values were in the range 0.602–17.578 MPa with mean of 3.137 MPa and standard deviation of 0.41 on the base-10 logarithmic scale. Thus, the stress drop of the Lushan earthquake could be taken as 3.137 MPa.
5. In some studies, the same value of stress drop has generally been employed for the EGF event and the target earthquake (e.g., Honoré et al. 2011; Sharma et al. 2013). Thus, the stress drop of the Lushan earthquake could be set to 2.049 MPa, i.e., the stress drop of the EGF event.

According to these various strategies, the estimated values of the stress drop of the Lushan earthquake are 1.5, 2.049, 2.31, 3.137, 3.60, 4.13, and 6.425 MPa and the corresponding values of C in

Table 1

Stress drop values ($\Delta\sigma_L$) estimated for the Lushan earthquake in accordance with various methods, and corresponding corner frequencies (f_{cL}), total source durations (T_c), and stress drop ratios (C) to the stress drop of the EGF event ($\Delta\sigma_S$)

$\Delta\sigma_L$ (MPa)	Method type for $\Delta\sigma_L$ estimation	Refs.	f_{cL} (Hz)	T_c (s)	$\Delta\sigma_S$ (MPa)	C
2.31	Eshelby method $\left(\Delta\sigma = \frac{7\pi^{3/2}}{16}\frac{M_0}{S^{3/2}}\right)^a$	Eshelby (1957), Somerville et al. (1999)	0.112	8.94	2.049	1.13
3.60	Eshelby method $\left(\Delta\sigma = \frac{7\pi^{3/2}}{16}\frac{M_0}{S^{3/2}}\right)^a$	Eshelby (1957), Wells and Coppersmith (1994)	0.130	7.71	2.049	1.76
4.13	Pulido method $\left(\Delta\sigma = M_0/0.229S^{3/2}\right)^a$	Pulido et al. (2004), Somerville et al. (1999)	0.136	7.36	2.049	2.02
6.425	Pulido method $\left(\Delta\sigma = M_0/0.229S^{3/2}\right)^a$	Pulido et al. (2004), Wells and Coppersmith (1994)	0.157	6.36	2.049	3.14
1.5	Dalguer method based on the aspect ratio of the ruptured plane	Dalguer et al. (2008)	0.097	10.32	2.049	0.73
3.137	Analogy method from the tectonic environment	Zafarani et al. (2012), Wen et al. (2015)	0.124	8.07	2.049	1.53
2.049	The same as that of the EGF event	Sharma et al. (2013)	0.107	9.30	2.049	1.0

M_0 and S represent the seismic moment calculated by the M_0–M_w relationship (Hanks and Kanamori 1979) and the total rupture area estimated using the empirical relationship between S and M_0 (or M_w) (Somerville et al. 1999; Wells and Coppersmith 1994)

Eq. (3) are 0.73, 1.0, 1.13, 1.53, 1.76, 2.02, and 3.14 (Table 1). The corresponding total rupture durations, which are represented by the inverse of the corner frequency based on the estimated stress drops, are in the range 6.36–10.32 s [Eq. (4)].

4. Ground-Motion Variability from Stochastic Rupture Process

Ground motions at 16 stations (Fig. 1), produced by the Lushan earthquake characterized by various stress drop values, are simulated using the stochastic EGF method. For each case of the seven estimations of stress drop mentioned above, 200 synthetics are obtained at each station according to 200 ESTFs generated stochastically, representing 200 stochastic rupture processes. Although acceleration time histories of the three basic components (east–west, north–south, and up–down) are all simulated for each station, we consider only the horizontal components in the present study. The horizontal 5%-damped pseudospectral acceleration (PSA), represented by the geometrical mean of the PSAs of both orthogonal horizontal components, is taken as the intensity measure of the simulated ground motion.

First, we discuss how much of the ground-motion variability is caused by the rupture process generated stochastically. The standard deviation of the horizontal PSAs on the base-10 logarithmic scale from the 200 stochastic rupture processes at each station is calculated for each case of seven stress drop values (or stress drop ratios). The mean of the standard deviations across all 16 stations for each case is shown in Fig. 2. It can be seen that the standard deviations in different cases show slight discrepancies, even if there is a very slight increasing tendency

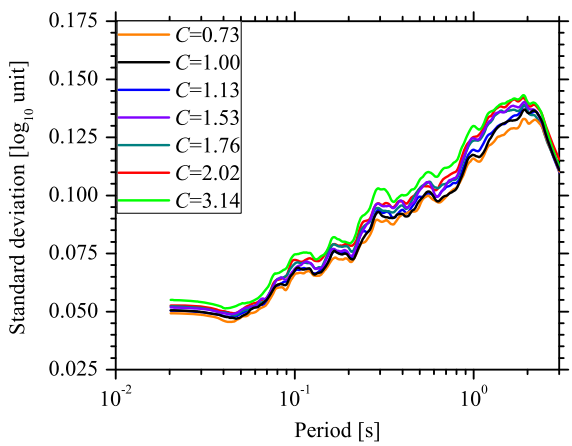

Figure 2
Mean of standard deviations of horizontal 5%-damped pseudospectral accelerations on base-10 logarithmic scale from 200 stochastic rupture processes across 16 stations considered in each case characterized by various stress drop ratios. The parameter C indicates the stress drop ratio between the target and EGF events

as the stress drop ratio increases. Salichon et al. (2010) also observed that the standard deviations of the spectral acceleration distributions from the stochastic EGF simulation remain fairly constant from one stress drop ratio to another. These results indicate that the variability of the simulated PSAs from the stochastic rupture processes is approximately independent of the selection of the value of the stress drop of the target earthquake, which implies that ground-motion variability arising from the stochastic rupture process is independent of that due to stress drop uncertainty. It can be seen that the standard deviation is approximately constant at 0.05 when the period is < 0.05 s. It then increases from $\sim$ 0.05 to $\sim$ 0.14 as the period increases from 0.05 to 2.0 s; however, it falls abruptly as the period increases from 2.0 to 3.0 s. The symbol τ' is used to represent the variability of the PSAs from the stochastic rupture process in this paper. τ' was regressed as a simple function of period (T) as

$$\tau' = 0.024 \cdot \ln(T) + 0.120 \text{ for } T = 0.05{-}2.0\,\text{s}. \quad (5)$$

It should be borne in mind that the randomness of the source rupture process in this study is established based on a particular symmetrical circular model, which is incapable of representing additional source complexity, e.g., in the source geometry, rupture directivity, and rupture speed (Kaneko and shearer 2014, 2015). The variability estimated from Eq. (5) is likely to be smaller in comparison with that for real earthquakes, even for small events. Our estimates are smaller than those ($\sim$ 0.075–0.2) reported by Causse et al. (2008) assuming a constant stress drop ratio of 1.0. They obtained their results from simulations using the classical EGF method (Irikura 1983) by considering a variety of source kinematic models with varies rupture velocities and nucleation locations on the ruptured fault to reflect the complex rupture process.

5. *Ground-Motion Variability Due to Stress Drop Uncertainty*

To investigate the ground-motion variability caused predominantly by stress drop uncertainty, we consider the average across the simulated PSAs from the stochastic rupture processes at each station for each case of the various stress drop ratios. The average or median of the PSAs from stochastic rupture processes is usually used to compare with the observation and prediction from GMPEs and to reflect the influence of stress drop on the simulated results (Courboulex et al. 2010; Honoré et al. 2011; Kohrs-Sansorny et al. 2005; Salichon et al. 2010). The average of the PSAs from the 200 stochastic rupture processes in each case of the various stress drop ratios is shown in Fig. 3 for all 16 stations considered. It is clear that the stress drop ratio exerts considerable influence on the synthetic results. The PSA level increases monotonically as the stress drop ratio increases, as also observed in previous studies (Honoré et al. 2011). It is deeply encouraging that observed PSAs are generally within the range of the PSAs simulated in the various cases. The mean of the average PSAs from the various cases can be in good agreement with the observation for up to half of all the stations considered, e.g., stations 051DJZ, 051XJD, 051JYW, and 051HSS. Hence, the blind ground-motion simulations for the Lushan earthquake can provide a satisfactory representation of the actual ground shaking in the frequency domain. However, the results are also disappointing, because it is rather difficult to clearly identify a uniform stress drop ratio from these values that results in the simulated PSAs always showing best agreement with the observations at all stations.

The PSA predictions derived from GMPEs, as shown in Fig. 3, are applied in an attempt at calibrating the appropriate stress drop ratio, as proposed by Courboulex et al. (2010). One GMPE applicable for the Sichuan–Yunnan region established by Wang et al. (2013b) (hereafter called the Wang13 model) and the widely used Next Generation Attenuation (NGA)-West2 models for global shallow crustal earthquakes (Abrahamson et al. 2014; Boore et al. 2014; Campbell and Bozorgnia 2014; Chiou and Youngs 2014; Idriss 2014) are considered in this study. The rupture distance and the Joyner–Boore distance used in the GMPEs are computed according to the finite rupture plane inverted by Wang et al. (2013a). The time-weighted average shear-wave velocity over the upper 30 m (V_{s30}) used in the NGA-West2 models is derived directly from the NGA site

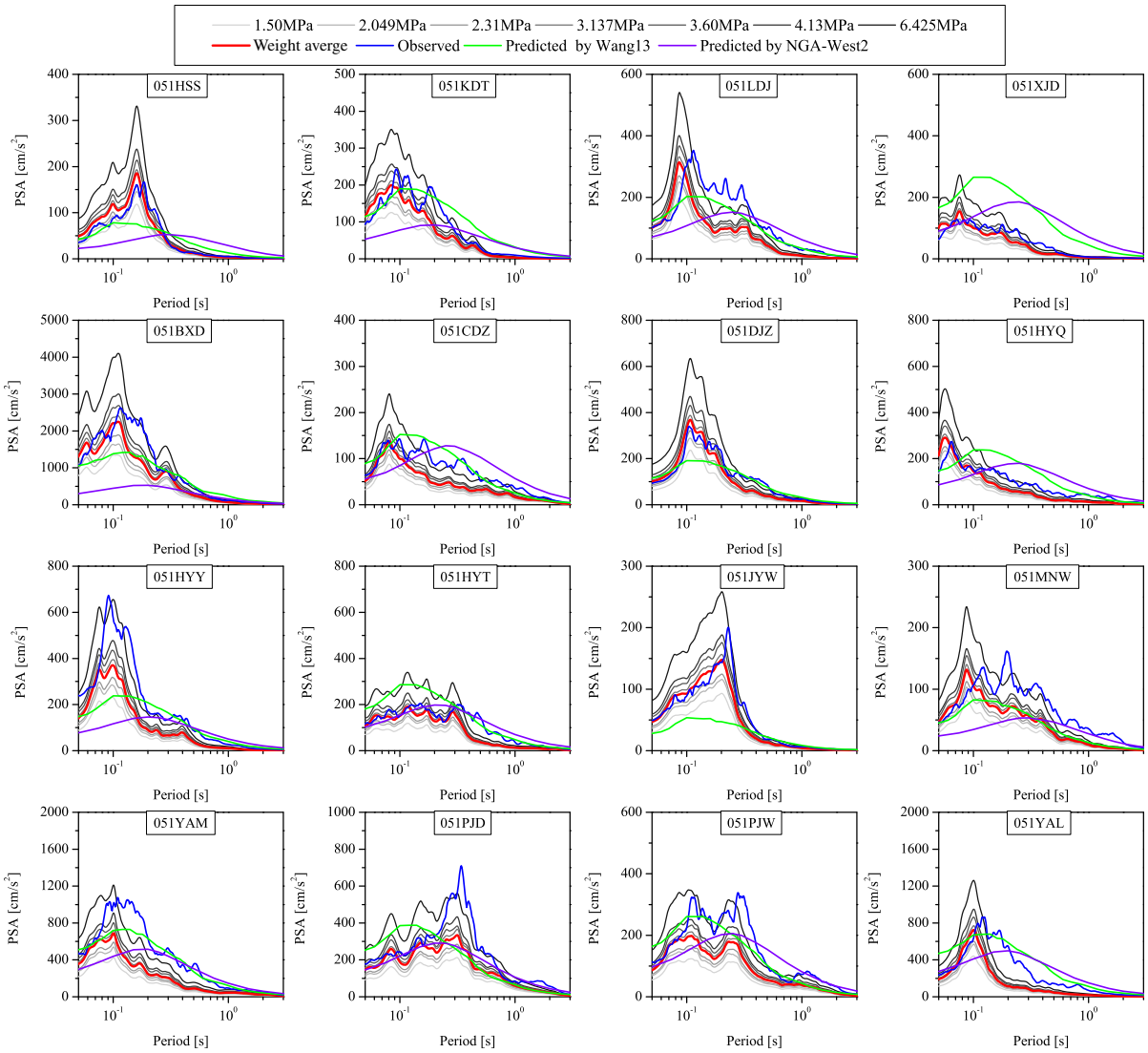

Figure 3

Horizontal 5%-damped pseudospectral accelerations (PSAs) of synthetic ground motions averaged across 200 stochastic rupture processes in each case with respect to various stress drop ratios compared with observed values. The equally weighted mean of the PSAs in the different cases at each station is plotted. Also plotted are predictions from two ground-motion prediction equations: one developed by Wang et al. (2013b) for the Sichuan–Yunnan region (Wang13 model) and the equally weighted Next Generation Attenuation (NGA)-West 2 models

database or inferred indirectly from the shear-wave velocity profile at depths of < 20 m, except for stations 051DJZ and 051JYW because of unavailable shear-wave velocity data. The NGA-West2 models are assigned equal weight to provide the mean prediction of PSA at a station. The PSA predictions derived from the Wang13 and NGA-West2 models show remarkable disagreement at almost all stations considered. The predictions from both models are in poor agreement with the simulations carried out in this study, as well as the observations. Even when supplemented by comparison with GMPEs, it remains difficult to make a reliable judgment regarding the stress drop ratio in the simulation that was optimal for representing the observations at all stations at the same time. These results strongly indicate that evaluation of ground-motion variability resulting from stress drop uncertainty is critical.

To eliminate the effects of other factors (e.g., propagation path and site) on ground motion and to place the spectral amplitudes at different stations on a comparable level, the normalized PSAs at each station (i.e., the ratios of synthetic PSAs for the case of $C = 1.0$ to those for cases of various values of C) are shown in Fig. 4. For a specific value of C, the normalized PSAs at all 16 stations show very slight differences but share the similar values at periods of 0.05–2.0 s. It is found that the scatter in the normalized PSAs among all stations gradually increases as the value of C increases. More importantly, slight dependence of the normalized PSAs on period is observed in the case of large values of C (e.g., $C = 3.14$). Therefore, the means of the normalized PSAs across all 16 stations at periods of 0.05–2.0 s (Fig. 4) are used to explore the potential relationship between ground motion and stress drop ratio (or stress drop).

As mentioned above, the stress drop values of the earthquakes in the Lushan seismic sequence provided by Wen et al. (2015) vary mainly in the range of 0.602–17.578 MPa. However, the stress drop values used lie in the relatively narrow range of 1.5–6.425 MPa. To elucidate the relationship between PSA and C, we expand the range of

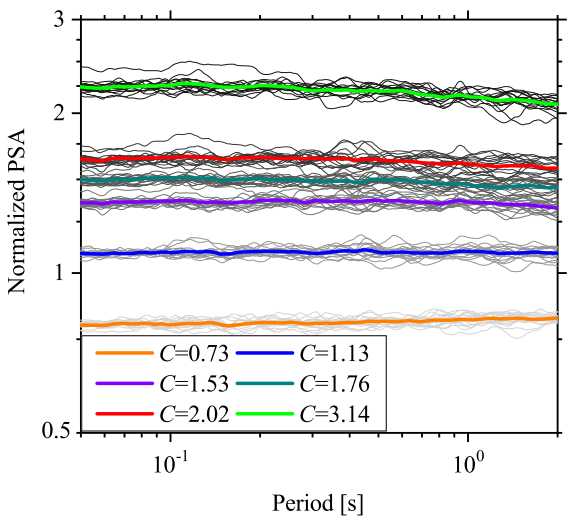

Figure 4
Synthetic PSAs at each station for various values of C, normalized by their respective synthetic PSA for the case of stress drop ratio (C) equal to 1.0. The mean of the normalized PSAs across all 16 stations in each case of a specific stress drop ratio is highlighted by a thick line

C values. Thus, this study considers the additional values of C of 0.24, 0.49, 4.88, 7.32, and 9.76, which correspond to stress drop values of 0.5, 1.0, 10, 15, and 20 MPa, respectively, for the Lushan earthquake. We simulate ground motions using the additional C values and calculate the normalized PSAs at each station.

The means of the normalized PSAs across all 16 stations at periods of 0.05–2.0 s versus the C value are plotted in Fig. 5a. It can be seen that the normalized PSAs increase as the value of C increases, as observed in Fig. 4, although the tendency of increase gradually slows. The normalized PSAs are approximately constant at periods of 0.05–2.0 s for cases of small values of C (i.e., $C < 4$). However, obvious dependence of the normalized PSAs on period can be observed for cases of large values of C (i.e., $C > 4$). The smaller normalized PSAs appear at longer periods, implying that the influence of the value of C is reasonably weak on long-period ground motion. The relationship between the normalized PSAs at a specific period (i) (hereafter represented by Y_i) and the C value can be expressed as

$$Y_i = aC^b, \tag{6}$$

where a and b are regression coefficients. Equation (6) can be transformed into a linear function on the logarithmic scale; thus, the $\ln(Y_i)$–$\ln(C)$ relationship at each period from 0.05 to 2.0 s is obtained by linear least-squares regression analysis. Coefficients a and b at each period are derived, as shown in Fig. 5b and c, respectively. It can be seen that coefficient a is approximately independent of the period, fluctuating slightly around a constant value of $\sim$ 1.0. However, the exponent b shows significant dependence on period, diminishing gradually from $\sim$ 0.71 to $\sim$ 0.62 as the period increases from 0.05 to 2.0 s. At very short periods, the value of b approximately converges to a constant of $\sim$ 0.7. A straightforward relationship between exponent b and period (T), applicable for the frequency band which is much beyond the corner frequency of the target event, can be expressed as

$$b = 0.702\ \exp(-0.062T) \text{ for } T = 0.05\text{–}2.0\,\text{s}. \tag{7}$$

The approximation of $Y_i = C^b$ arises from Eq. (6) because of the approximately constant value of a of

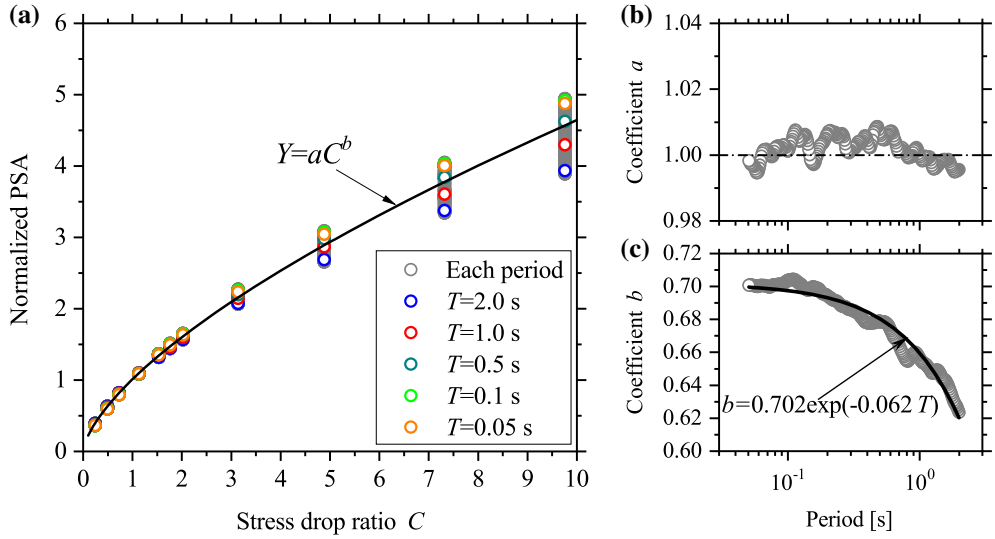

Figure 5

a Means of normalized PSAs across all 16 stations considered at periods of 0.05–2.0 s versus the stress drop ratio C. The relationship between the mean of the normalized PSAs at a specific period (represented as Y) and the value of C is represented by a solid line based on the functional form $Y = aC^b$. Coefficients a and b in the Y–C relationship at periods of 0.05–2.0 s, derived by least-squares regression analysis, are shown in **b** and **c**, respectively

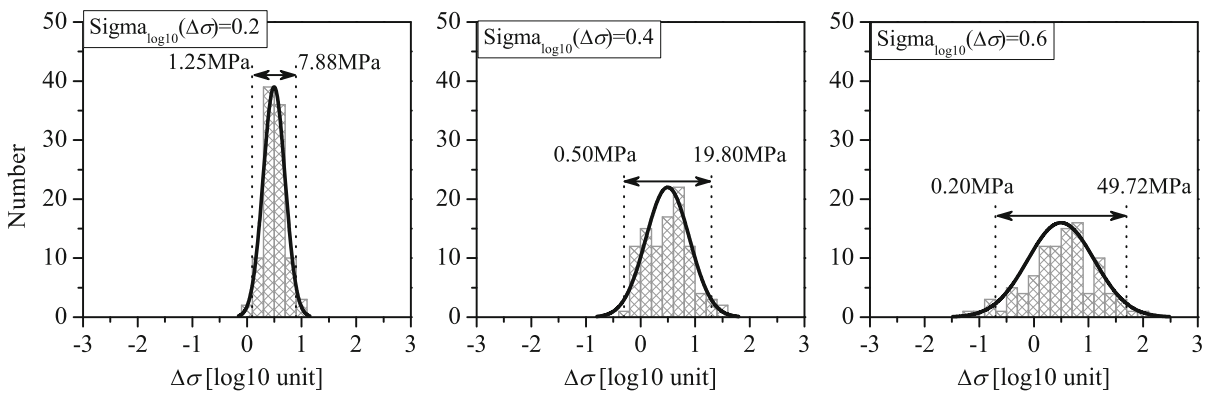

Figure 6

Histograms of stress drops from three collections generated randomly by the Monte Carlo sampling technique. Overall, 100 random values following a lognormal distribution are included in each collection. The mean is fixed to 3.137 MPa, and the standard deviation is variable, i.e., 0.2, 0.4, and 0.6 for each of the three collections. The arrowed lines represent the 97.5th to 2.5th percentiles corresponding to the mean ± 1.96 standard deviations

$\sim$ 1. Y indirectly represents the synthetic ground motion, and C is proportional to the stress drop of the target event given that the stress drop value of the EGF event is determined. Hence, the synthetic PSA is proportional to $\Delta\sigma^b$, i.e., PSA $\sim$ $\Delta\sigma^b$. Following this scaling, the variability of synthetic ground motion [hereafter, represented as $\mathrm{Sigma}_{\log 10}(\mathrm{PSA})$, i.e., the standard deviation of PSA on the base-10 logarithmic scale] resulting purely from the variability of the stress drop [denoted as $\mathrm{Sigma}_{\log 10}(\Delta\sigma)$, i.e., the standard deviation of the stress drop on the base-10 logarithmic scale] can be expressed as

$$\mathrm{Sigma}_{\log 10}(\mathrm{PSA}) = b\mathrm{Sigma}_{\log 10}(\Delta\sigma). \quad (8)$$

Assuming $\mathrm{PSA}_{T\to 0}$ = PGA, b is equal to 0.702 for PGA. This result is smaller than the value of 5/6

given by Cotton et al. (2013) based on a theoretical expression for the stress drop (Brune 1970) and the root-mean-square acceleration (a_{rms}) expressed as a function of stress drop (McGuire and Hanks 1980). In the study of Cotton et al. (2013), it was assumed that the τ of the PGA reported in the GMPE was dominated entirely by $\mathrm{Sigma}_{\log 10}(\Delta\sigma)$. Actually, τ reflects the ground-motion variability induced by event-to-event variations that are not accounted for by the magnitude, style of fault, and source depth considered in the GMPE. Although the stress drop is one of the key factors in relation to τ, it is not the only one; therefore, a value of b larger than ours was used in their study to explain the value of τ. In the study of Baltay et al. (2013), they investigated the variability of stress drop, both $\Delta\sigma$-EGF (determined by the corner frequency and seismic moment based on the EGF method) and $\Delta\sigma$-a_{rms} (determined by the a_{rms} of the near-field ground motion). The similar variability between $\Delta\sigma$-EGF and $\Delta\sigma$-a_{rms} suggested that the variability in stress drop stems from the interevent source variability. They concluded that the variability in stress drop can be regarded as a bound on the interevent standard deviation in GMPEs. The interevent standard deviation must be higher than the ground-motion variability purely caused by the variability in stress drop. It is the same for the variability in stress drop due to the smaller b values (< 1.0). We infer that the variability in stress drop may represent approximately the interevent standard deviation in GMPEs, which is similar to the conclusion of Baltay et al. (2013).

The stress drop values of the Lushan earthquake are then set to collections of random samples, and additional simulations based on random stress drop values produced to verify the reliability of the relationship between ground-motion variability and stress drop uncertainty. The random samples in each collection follow a lognormal distribution with average of 3.137 MPa, i.e., the mean stress drop value of the earthquakes in the Lushan seismic sequence (Wen et al. 2015). However, the standard deviation of the random samples, $\mathrm{Sigma}_{\log 10}(\Delta\sigma)$, is a variable, increasing monotonically from 0.1 to 0.6 in constant intervals of 0.05. The Monte Carlo sampling technique is adopted to generate 100 random samples for each of the 11 collections. The histograms of the random samples in three collections with standard deviation of 0.2, 0.4, and 0.6 are shown in Fig. 6, revealing that the random samples match the lognormal distribution well. The random stress drop values in the collection with the largest standard deviation (0.6) exhibit large scatter, with variations on the order of 10^3. These random values showing small standard deviation (0.2) still vary by a factor of 10 or more.

The stochastic EGF method is now used to obtain 200 synthetics for each station produced by the Lushan earthquake characterized by various random stress drops. The mean of the simulated PSAs from the 200 stochastic rupture processes is regarded as the ground-motion intensity for a specific stress drop value. The variability of the simulated ground motions resulting from 100 random stress drop values in each collection, denoted by $\mathrm{Sigma}_{\log 10}(\mathrm{PSA})$, is calculated at each station. The ratios of $\mathrm{Sigma}_{\log 10}(\mathrm{PSA})$ to $\mathrm{Sigma}_{\log 10}(\Delta\sigma)$ are plotted in Fig. 7.

For a specific $\mathrm{Sigma}_{\log 10}(\Delta\sigma)$ value, the resulting ratios do not show significant discrepancies at different stations. The ratios mainly vary in the range of ~ 0.7 to ~ 0.6. Obviously, a downwards trend of the ratio is observed as the period increases from 0.05 to 2.0 s for all cases of $\mathrm{Sigma}_{\log 10}(\Delta\sigma)$ considered, which indicates smaller variability in long-period ground motions due to stress drop uncertainty. The ratio correlated strongly to period can be expressed in the following functional form, similar to that in Eqs. (7) and (8):

$$\mathrm{Sigma}_{\log 10}(\mathrm{PSA})/\mathrm{Sigma}_{\log 10}(\Delta\sigma) = p\exp(qT). \tag{9}$$

Based on least-squares regression analysis, coefficients p and q in Eq. (9) for each case of $\mathrm{Sigma}_{\log 10}(\Delta\sigma)$ value are calculated and plotted in Fig. 8. The values of coefficient p are approximately constant, i.e., always equal to ~ 0.7 for various $\mathrm{Sigma}_{\log 10}(\Delta\sigma)$ values. Similarly, the values of coefficient q are also close to a constant value for $\mathrm{Sigma}_{\log 10}(\Delta\sigma) \geq 0.2$, i.e., approximately -0.06, whereas much greater values are observed for $\mathrm{Sigma}_{\log 10}(\Delta\sigma) < 0.2$, i.e., ~ -0.04 for $\mathrm{Sigma}_{\log 10}(\Delta\sigma) = 0.1$. Coefficients p and q are both in good agreement with those in Eq. (7), further

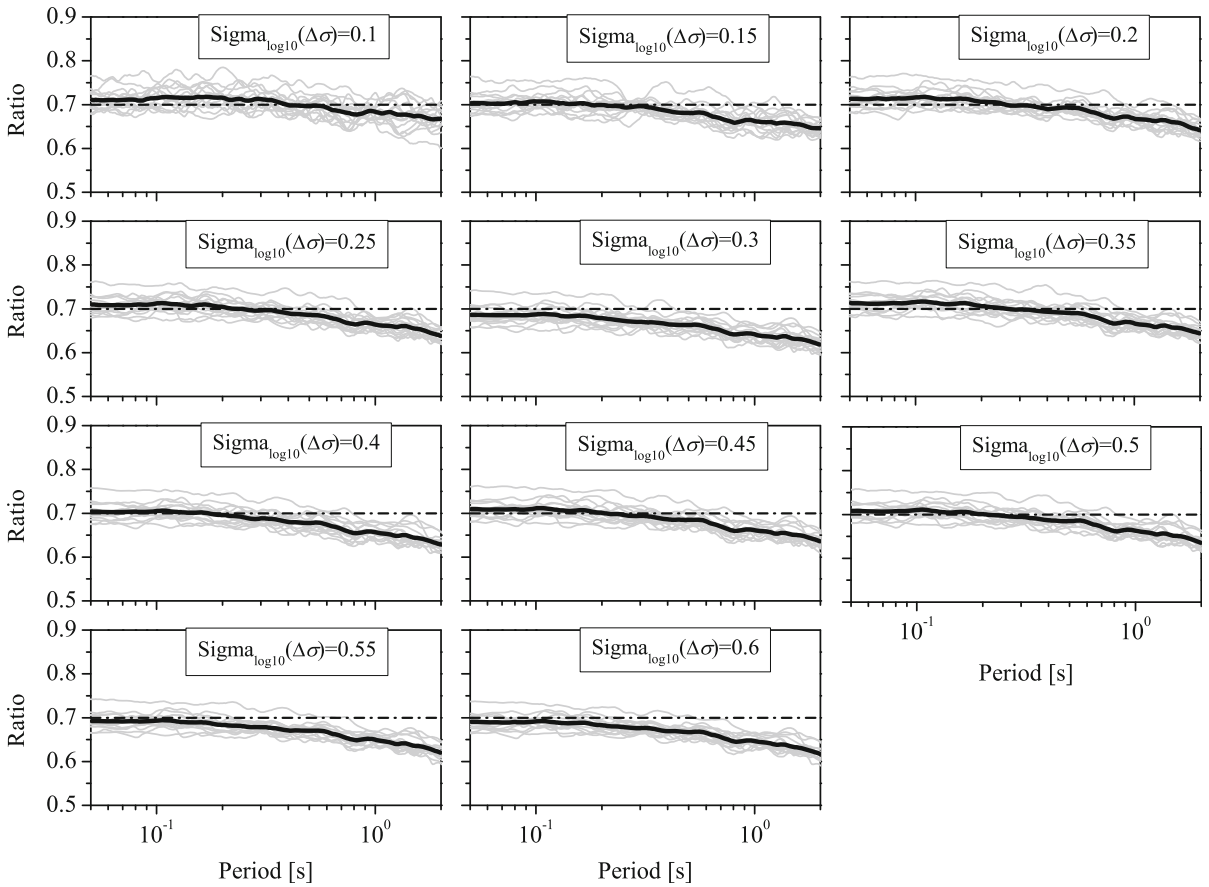

Figure 7
Ratios of $Sigma_{log10}(PSA)$ to $Sigma_{log10}(\Delta\sigma)$ at each station for cases of various values of $Sigma_{log10}(\Delta\sigma)$. The black solid line represents the mean across all 16 stations

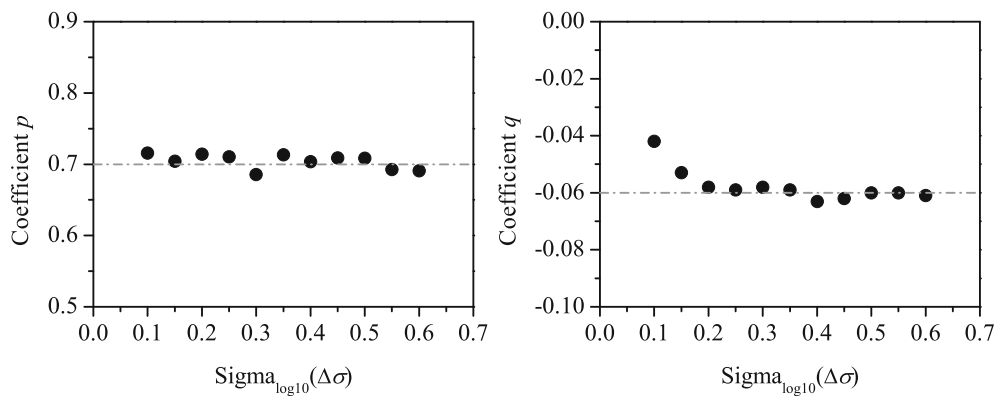

Figure 8
Coefficients p and q in Eq. (9) derived based on least-squares regression analysis for various values of $Sigma_{log10}(\Delta\sigma)$

confirming the reliability of the relationship between ground-motion variability and stress-drop variability.

6. Standard Deviation of Stress Drop

As described in Eq. (5) and Fig. 2, the role of the variability of a stochastic rupture process in ground-motion variability is not negligible. In this study, we assume that the interevent standard deviation of ground motion is constrained totally by the stress drop and the rupture process. Considering the independence of ground-motion variability from the stress-drop variability and the stochastic rupture process, the interevent standard deviation of ground motion can be expressed as the vector superposition of the ground-motion variability from the stress drop and the rupture process, i.e.,

$$\tau = \sqrt{\tau'^2 + \left[b\mathrm{Sigma}_{\log 10}(\Delta\sigma)\right]^2}. \qquad (10)$$

The stress-drop variability can be expressed as

$$\mathrm{Sigma}_{\log 10}(\Delta\sigma) = \sqrt{\tau^2 - \tau'^2}/b. \qquad (11)$$

The representations of τ' and b are described in detail in relation to Eqs. (5) and (7), respectively. Assuming $\mathrm{PSA}_{T\to 0} = \mathrm{PGA}$, then $\tau' = 0.05$ and $b = 0.702$. Estimations of $\mathrm{Sigma}_{\log 10}(\Delta\sigma)$ from Eq. (11) are $\sim$ 1.03–1.16 times larger than provided by Cotton et al. (2013) based on the interevent standard deviations of the PGAs reported for various GMPEs, listed in Table 1 in their study.

According to Eq. (11), $\mathrm{Sigma}_{\log 10}(\Delta\sigma)$ values can be derived from the τ values in the GMPEs for shallow crustal earthquakes across broad regions, as shown in Fig. 9. Some GMPEs developed for various regions have been adopted to retrieve $\mathrm{Sigma}_{\log 10}(\Delta\sigma)$ values, including the Bin11 model for Italy (Bindi et al. 2011), Wang13 model for the Sichuan–Yunnan region in China (Wang et al. 2013b), Wen18 model for the Sichuan region in China (Wen et al. 2018), BSSA14 model (Boore et al. 2014), ASK14 model (Abrahamson et al. 2014), and CB14 model (Campbell and Bozorgnia 2014) for global shallow crustal earthquakes, Zhao06 model for Japan (Zhao et al. 2006), and Kale15 model for Turkey and Iran (Kale et al. 2015). In the BSSA14, ASK14, CB14, and Kale15 models, magnitude-dependent τ values were provided. In this study, we adopt the τ values for $M_w \le 4.5$ in the BSSA14 model, $M_w < 5$ in the ASK14 model, $M_w \le 4.5$ in the CB14 model, and $M_w < 6.0$ in the Kale15 model. The τ values in these GMPEs vary mainly in the range 0.15–0.25 on the base-10 logarithmic scale. It was found that the $\mathrm{Sigma}_{\log 10}(\Delta\sigma)$ values varied with period and were different among the different GMPEs. In general, the $\mathrm{Sigma}_{\log 10}(\Delta\sigma)$ estimations varied mainly in the range 0.20–0.30. The contribution of the variability in stress drop to the total interevent standard deviation of PSA at period of 0.05 s in GMPEs accounts for approximately 55–67% according to the $\mathrm{Sigma}_{\log 10}(\Delta\sigma)$ estimations. It is found that the contribution decreases gradually as the period increases from 0.05 to 2.0 s.

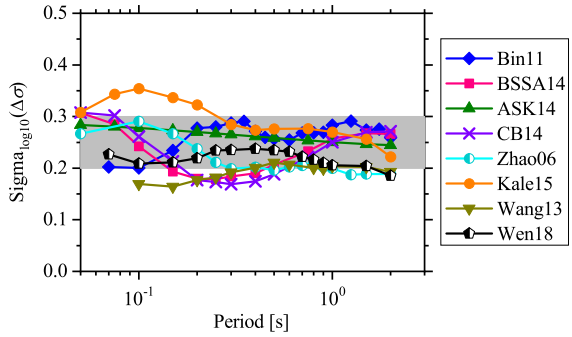

Figure 9
Variability in stress drop, denoted by $\mathrm{Sigma}_{\log 10}(\Delta\sigma)$, retrieved from the interevent standard deviations reported for GMPEs established for various regions. The shaded area indicates the main range of the $\mathrm{Sigma}_{\log 10}(\Delta\sigma)$ values estimated in this study

The stress-drop variability derived from earthquake source studies using different measurement methods (e.g., isolating source displacement spectra, nonparametric spectral inversion, determining STF duration from the SCARDEC, EGF method) is listed in Table 2 for comparison with our estimations. Our results indicate that stress-drop variability driven by the observed ground-motion data is generally smaller than that derived from earthquake source studies, e.g., 0.48 for crustal earthquakes in Japan (Oth et al. 2017), 0.43 and 0.45 for global subduction and non-subduction shallow earthquakes, respectively (Courboulex et al. 2016), and 0.48 for crustal earthquakes during the last 10 years in central Italy (Bindi

Table 2

Stress-drop variability obtained from earthquake source studies and this study

Study	Region	$\text{Sigma}_{\log10}(\Delta\sigma)$	No. of earthquakes
This study	Shallow crustal earthquakes	0.20–0.30	
Allmann and Shearer (2009)	Subduction	0.21	481
Allmann and Shearer (2009)	Oceanic ridge boundary	0.48	23
Allmann and Shearer (2009)	Oceanic transform fault	0.68	115
Allmann and Shearer (2009)	Oceanic collision boundary	0.56	25
Allmann and Shearer (2009)	Continental ridge boundary	0.47	26
Allmann and Shearer (2009)	Continental transform fault	0.64	48
Allmann and Shearer (2009)	Continental collision boundary	0.5	81
Allmann and Shearer (2009)	Intraplate	1.01	61
Courboulex et al. (2016)	Subduction interface $M_w > 5.8$	0.43	313
Courboulex et al. (2016)	Outside subduction interface $M_w > 5.8$	0.45	347
Oth et al. (2017)	Japan (crustal) M_w = 2.7–7.2	0.48	1905
Bindi et al. (2018)	Central Italy M_w = 2.5–6.5	0.45	1400
Wang et al. (2018)	2008 Wenchuan seismic sequence M_w = 3.50–6.12	0.28	132
Baltay et al. (2011)	2004 Chuetsu, 2007 Chuetsu-Oki, 2008 Iwate-Miyagi Nairiku, and 2008 Kamaishi earthquake sequences	0.40	90

et al. 2018). Even for the same Sichuan region, the estimated stress-drop variability ($\sim$ 0.20–0.25) from the Wen18 model (Wen et al. 2018) developed using strong-motion data mostly from the Wenchuan earthquake sequence is still smaller than that of the Wenchuan earthquake sequence (0.28) estimated by Wang et al. (2018) using the spectral inversion method. However, the aleatory uncertainty of the stress drop calculated by Causse et al. (2014) using 31 kinematic inversion models of 21 crustal earthquakes (M_w 5.7–7.7), $\sim$ 0.3 (log10 units) is slightly higher than our estimates.

7. Conclusions

Using the stochastic EGF method, we simulate ground motions produced by the 2013 M_w6.6 Lushan earthquake, characterized by various stress drop values estimated from different approaches. We first investigate ground-motion variability arising from the stochastic rupture process in this simulation method. The resulting $\text{Sigma}_{\log10}$(PSA) is found to increase from $\sim$ 0.05 to $\sim$ 0.14 as the period increases to 2.0 s, being independent of the stress drop of the target earthquake considered. This implies that ground-motion variability from the stochastic rupture process and stress drop uncertainty is approximately independent.

The ground-motion variability arising purely from the stress drop uncertainty is also investigated. A significant effect of stress drop on the simulated ground motions is clearly observed; i.e., higher stress drop led to greater PSA. It was found that the spectral amplitude is approximately linearly proportional to the stress drop with a power of exponent b. The b value derived based on a regression analysis is found to be strongly dependent on period, decreasing from $\sim$ 0.7 to $\sim$ 0.6 as the period increases from 0.05 to 2.0 s and converging to $\sim$ 0.7 at very short periods. Based on the linear relationship between PSA and stress drop on the logarithmic scale, we conclude that the standard deviation of stress drop is linearly correlated to the standard deviation of ground motion, i.e., $\text{Sigma}_{\log10}(\text{PSA}) = b\text{Sigma}_{\log10}(\Delta\sigma)$. Moreover, the ground-motion variability, calculated directly from simulations based on collections of random stress drops with various standard deviations, verifies the reliability of the relationship between ground-motion variability and stress-drop variability. The b value derived in this study explains how much of the ground-motion variability is caused purely by the stress drop uncertainty. We expect further roles for the b value in seismic hazard analysis.

Assuming that the interevent standard deviation of GMPEs is controlled entirely by the stress drop uncertainty and the stochastic rupture process, some GMPEs for broad regions are considered to assess the variability of the stress drop. In general, the derived values of $\mathrm{Sigma}_{\log 10}(\Delta\sigma) = \sim 0.2$–$0.3$ are found to be significantly smaller than those derived from M_0–f_c analyses of earthquake source spectra. The contribution of the stress-drop variability to the total interevent standard deviation decreases gradually as the period increases from 0.05 s to 2.0 s. The contribution to the total interevent standard deviation of PSA at period of 0.05 s in GMPEs accounts for approximately 55–67%. Reasonable consideration of the stress drop in ground-motion models will be an efficient way to depress ground-motion uncertainty.

Acknowledgements

Strong-motion recordings used in this article were collected by the China Strong-Motion Network Center. Due to the current maintenance of its website (http://www.csmnc.net/) (official notice of Institute of Engineering Mechanics, CEA can be obtained at http://www.iem.ac.cn/detail.thml?id=1102), we contacted the email csmnc@iem.ac.cn for data application (last accessed June 2017). Basic information (surface wave magnitude, hypocentral location) on earthquakes was derived from the China Earthquake Network Center at website http://news.ceic.ac.cn/ (last accessed June 2017). The V_{S30} measurements for some stations were derived from the Next Generation Attenuation (NGA) site database of the Pacific Earthquake Engineering Research Center and are available for download at http://peer.berkeley.edu/nga/ (last accessed June 2017). This work was supported by the National Key R&D Program of China (no. 2017YFC1500801), National Natural Science Foundation of China (nos. 51808514 and 51878632), Natural Science Foundation of Heilongjiang Province (no. E2017065), and Science Foundation of the Institute of Engineering Mechanics, China Earthquake Administration (no. 2018B03). We sincerely appreciate the three anonymous reviewers for their valuable comments.

References

Abercrombie, R. E. (2015). Investigating uncertainties in empirical Green's function analysis of earthquake source parameters. *Journal of Geophysical Research: Solid Earth*. https://doi.org/10.1002/2015JB011984.

Abrahamson, N. A., Silva, W. J., & Kamai, R. (2014). Summary of the ASK14 ground motion relation for active crustal regions. *Earthquake Spectra, 30*(3), 1025–1055. https://doi.org/10.1193/070913EQS198M.

Allmann, B. P., & Shearer, P. M. (2009). Global variations of stress drop for moderate to large earthquakes. *Journal of Geophysical Research, 114,* B01310. https://doi.org/10.1029/2008JB005821.

Baltay, A. S., & Hanks, T. C. (2014). Understanding the magnitude dependence of PGA and PGV in NGA-West2 data. *Bulletin of the Seismological Society of America, 104*(6), 2851–2865. https://doi.org/10.1785/0120130283.

Baltay, A. S., Hanks, T. C., & Beroza, G. C. (2013). Stable stress-drop measurements and their variability: implications for ground-motion prediction. *Bulletin of the Seismological Society of America, 103*(1), 211–222. https://doi.org/10.1785/0120120161.

Baltay, A., Ide, S., Prieto, G., & Beroza, G. (2011). Variability in earthquake stress drop and apparent stress. *Geophysical Research Letters, 38,* L06303. https://doi.org/10.1029/2011GL046698.

Beauval, C., Honoré, L., & Courboulex, F. (2009). Ground-motion variability and implementation of a probabilistic-deterministic hazard method. *Bulletin of the Seismological Society of America, 99*(5), 2992–3002. https://doi.org/10.1785/0120080183.

Bindi, D., Pacor, F., Luzi, L., Puglia, R., Massa, M., Ameri, G., et al. (2011). Ground motion prediction equations derived from the Italian strong motion database. *Bulletin of Earthquake Engineering, 9,* 1899–1920. https://doi.org/10.1007/s10518-011-9313-z.

Bindi, D., Spallarossa, D., Picozzi, M., Scafidi, D., & Cotto, F. (2018). Impact of magnitude selection on aleatory variability associated with ground-motion prediction equations: part I—local, energy, and moment magnitude calibration and stress-drop variability in central Italy. *Bulletin of the Seismological Society of America, 108*(3A), 1427–1442. https://doi.org/10.1785/0120170356.

Bjerrum, L. W., Sørensen, M. B., Ottemöller, L., & Atakan, K. (2013). Ground motion simulations for İzmir, Turkey: parameter uncertainty. *Journal of Seismology, 17*(4), 1223–1252. https://doi.org/10.1007/s10950-013-9389-9.

Boore, D. M. (2003). Simulation of ground motion using stochastic method. *Pure and Applied Geophysics*, *160*, 635–676. https://doi.org/10.1007/PL00012553.

Boore, D. M., Stewart, J. P., Seyhan, E., & Atkinson, G. M. (2014). NGA-West2 equations for predicting PGA, PGV, and 5% damped PSA for shallow crustal earthquakes. *Earthquake Spectra, 30*(3), 1057–1085. https://doi.org/10.1193/070113EQS184M.

Brune, J. (1970). Tectonic stress and the spectra of seismic shear waves from earthquakes. *Journal of Geophysical Research, 75,* 4997–5009. https://doi.org/10.1029/JB075i026p04997.

Campbell, K. W., & Bozorgnia, Y. (2014). NGA-West2 ground motion model for the average horizontal components of PGA, PGV, and 5% damped linear acceleration response spectra. *Earthquake Spectra, 30*(3), 1087–1115. https://doi.org/10.1193/062913EQS175M.

Causse, M., Cotton, F., Cornou, C., & Bard, P.-Y. (2008). Calibrating median and uncertainty estimations for a practical use of empirical Green's functions technique. *Bulletin of the Seismological Society of America, 98*(1), 344–353. https://doi.org/10.1785/0120070075.

Causse, M., Dalguer, L. A., & Mai, P. M. (2014). Variability of dynamic source parameters inferred from kinematic models of past earthquakes. *Geophysical Journal International, 196,* 1754–1769. https://doi.org/10.1093/gji/ggt478.

Causse, M., & Song, S. G. (2015). Are stress drop and rupture velocity of earthquakes independent? Insight from observed ground motion variability. *Geophysical Research Letters*. https://doi.org/10.1002/2015GL064793.

Chiou, B. S.-J., & Youngs, R. R. (2014). Update of the Chiou and Youngs NGA model for the average horizontal component of peak ground motion and response spectra. *Earthquake Spectra, 30*(3), 1117–1153. https://doi.org/10.1193/072813EQS219M.

Cocco, M., Tinti, E., & Cirella, A. (2016). On the scale dependence of earthquake stress drop. *Journal of Seismology, 20,* 1151–1170. https://doi.org/10.1007/s10950-016-9594-4.

Cotton, F., Archuleta, R., & Causse, M. (2013). What is sigma of the stress drop? *Seismological Research Letters, 84*(1), 42–48. https://doi.org/10.1785/0220120087.

Courboulex, F., Converset, J., Balestram, J., & Delouis, B. (2010). Ground-motion simulations of the 2004 M_w 6.4 Les Saintes, Guadeloupe, earthquake using ten smaller events. *Bulletin of the Seismological Society of America, 100*(1), 116–130. https://doi.org/10.1785/0120080372.

Courboulex, F., Vallée, M., Causse, M., & Chounet, A. (2016). Stress-drop variability of shallow earthquakes extracted from a global database of source time functions. *Seismological Research Letters, 87*(4), 912–918. https://doi.org/10.1785/0220150283.

Dalguer, L. A., Miyake, H., Day, S. M., & Irikura, K. (2008). Surface rupturing and buried dynamic-rupture models calibrated with statistical observations of past earthquakes. *Bulletin of the Seismological Society of America, 98*(3), 1147–1161. https://doi.org/10.1785/0120070134.

Das, S., & Kostrov, B. V. (1986). Fracture of a single asperity on a finite fault: a model for weak earthquakes? *Earthquake Source Mechanism* (pp. 91–96). Washington: America Geophysical Union.

Eshelby, J. D. (1957). The determination of the elastic field of an ellipsoidal inclusion, and related problems. *Proceedings of the Royal Society, 241*(1226), 376–396. https://doi.org/10.1098/rspa.1957.0133.

Hao, J., Ji, C., Wang, W., & Yao, Z. (2013). Rupture history of the 2013 M_w6.6 Lushan earthquake constrained with local strong motion and teleseismic body and surface waves. *Geophysical Research Letters, 40,* 5371–5376. https://doi.org/10.1002/2013GL056876.

Hanks, T. C., & Kanamori, H. (1979). A moment magnitude scale. *Journal of Geophysical Research*, *84*, 2348–2350.

Honoré, L., Courboulex, F., & Souriau, A. (2011). Ground motion simulations of a major historical earthquake (1660) in the French Pyrenees using recent moderate size earthquakes. *Geophysical Journal International, 187,* 1001–1018. https://doi.org/10.1111/j.1365-246X.2011.05319.x.

Idriss, I. M. (2014). An NGA-West3 empirical model for estimating the horizontal spectra values generated by shallow crustal earthquakes. *Earthquake Spectra, 30*(3), 1155–1177. https://doi.org/10.1193/070613EQS195M.

Irikura, K. (1983). Semi-empirical estimation of strong ground motions during large earthquake. *Bulletin of the Disaster Prevention Research Institute, Kyoto University, 33*(Part 2), 298.

Kale, Ö., Akkar, S., Ansari, A., & Hamzehloo, H. (2015). A ground-motion predictive model for Iran and Turkey for horizontal PGA, PGV, and 5% damped response spectrum: investigation of possible regional effects. *Bulletin of the Seismological Society of America, 105*(2A), 963–980. https://doi.org/10.1785/0120140134.

Kanamori, H. (1994). Mechanics of earthquakes. *Annual Review of Earth and Planetary Sciences, 22,* 207–237.

Kanamori, H., & Anderson, D. L. (1975). Theoretical basis of some empirical relations in seismology. *Bulletin of the Seismological Society of America, 65*(5), 1073–1095.

Kaneko, Y., & Shearer, P. M. (2014). Seismic source spectra and estimated stress drop derived from cohesive-zone models of circular subshear rupture. *Geophysical Journal International, 197,* 1002–1015. https://doi.org/10.1093/gji/ggu030.

Kaneko, Y., & Shearer, P. M. (2015). Variability of seismic source spectra, estimated stress drop, and radiated energy, derived from cohesive-zone models of symmetrical and asymmetrical circular and elliptical ruptures. *Journal of Geophysical Research: Solid Earth*. https://doi.org/10.1002/2014JB011642.

Kohrs-Sansorny, C., Courboulex, F., Bour, M., & Anne, D. (2005). A two-stage method for ground-motion simulation using stochastic summation of small earthquakes. *Bulletin of the Seismological Society of America, 95*(4), 1387–1400. https://doi.org/10.1785/0120040211.

Lyu, J., Wang, X. S., Su, J. R., Pan, S. L., Li, Z., Yin, L. W., et al. (2013). Hypocenter location and source mechanism of the M_s 7.0 Lushan earthquake sequence. *Chinese Journal of Geophysics, 56*(5), 1753–1763. https://doi.org/10.6038/cjg20130533. **(in Chinese)**.

Madariaga, R. (1976). Dynamics of an expanding circular fault. *Bulletin of the Seismological Society of America*, *66*(3), 639–666.

McGuire, R. K., & Hanks, T. C. (1980). RMS accelerations and spectral amplitudes of strong motion during the San Fernando earthquake. *Bulletin of the Seismological Society of America, 70*(5), 1907–1920.

Oth, A., Miyake, H., & Bindi, D. (2017). On the relation of earthquake stress drop and ground motion variability. *Journal of Geophysical Research: Solid Earth, 122,* 5474–5492. https://doi.org/10.1002/2017JB014026.

Pulido, N., Ojeda, A., Atakan, K., & Kubo, T. (2004). Strong ground motion estimation in the Sea of Marmara region (Turkey) based on a scenario earthquake. *Tectonophysics, 391,* 357–374. https://doi.org/10.1016/j.tecto.2004.07.023.

Salichon, J., Kohrs-Sansorny, C., Bertrand, E., & Courboulex, F. (2010). A M_w6.3 earthquake scenario in the city of Nice (southeast France): ground motion simulations. *Journal of Seismology, 14*(3), 523–541. https://doi.org/10.1007/s10950-009-9180-0.

Sharma, B., Chopra, S., Sutar, A. K., & Bansal, B. K. (2013). Estimation of strong ground motion from a great earthquake M_w 8.5 in central seismic gap region, Himalaya (India) using empirical Green's function technique. *Pure and Applied Geophysics, 170*(12), 2127–2138. https://doi.org/10.1007/s00024-013-0647-0.

Somerville, P., Irikura, K., Graves, R., Sawada, S., Wald, D., Abrahamson, N., et al. (1999). Characterizing crustal earthquake slip models for the prediction of strong ground motion. *Seismological Research Letters, 70*(1), 59–70.

Sørensen, M. B., Pulidu, N., & Atakan, K. (2007). Sensitivity of ground-motion simulations to earthquake source parameters: a case study for Istanbul, Turkey. *Bulletin of the Seismological Society of America, 97*(3), 881–900. https://doi.org/10.1785/0120060044.

Wang, W. M., Hao, J. L., & Yao, Z. X. (2013a). Preliminary result for rupture process of Apr. 20, 2013, Lushan earthquake, Sichuan, China. *Chinese Journal of Geophysics, 56*(4), 1412–1417. https://doi.org/10.6038/cjg20130436. **(in Chinese)**.

Wang, Y. S., Li, X. J., & Zhou, Z. H. (2013b). Research on attenuation relationships for horizontal strong ground motions in Sichuan-Yunnan region. *Acta Seismologica Sinica, 35*(2), 238–249. **(in Chinese)**.

Wang, H. W., Ren, Y. F., & Wen, R. Z. (2018). Source parameters, path attenuation and site effects from strong-motion recordings of the Wenchuan aftershocks (2008–2013) using a non-parametric generalized inversion technique. *Geophysical Journal International, 212,* 872–890. https://doi.org/10.1093/gji/ggx447.

Wang, H. W., Wen, R. Z., & Ren, Y. F. (2017). Simulating ground-motion directivity using stochastic empirical Green's function method. *Bulletin of the Seismological Society of America, 107*(1), 359–371. https://doi.org/10.1785/0120160083.

Wells, D. L., & Coppersmith, K. J. (1994). New empirical relationships among magnitude, rupture length, rupture width, rupture area, and surface displacement. *Bulletin of the Seismological Society of America, 84*(4), 974–1002.

Wen, R. Z., Wang, H. W., & Ren, Y. F. (2015). Estimation of source parameters and quality factor based on the generalized inversion method in Lushan earthquake. *Journal of Harbin Institute of Technology, 47*(4), 58–63. https://doi.org/10.11918/j.issn.0367-6234.2015.04.010. **(in Chinese)**.

Wen, R. Z., Xu, P. B., Wang, H. W., & Ren, Y. F. (2018). Single-station standard deviation using strong-motion data from the Sichuan region, China. *Bulletin of the Seismological Society of America, 108*(4), 2237–2247. https://doi.org/10.1785/0120170276.

Zafarani, H., Vahidifard, H., & Ansari, A. (2012). Sensitivity of ground-motion scenarios to earthquake source parameters in the Tehran metropolitan area, Iran. *Soil Dynamics and Earthquake Engineering, 43,* 342–354. https://doi.org/10.1016/j.soildyn.2012.07.007.

Zhang, Y., Wang, R., Chen, Y. T., Xu, L., Du, F., Jin, M., et al. (2014). Kinematic rupture model and hypocenter relocation of the 2013 M_w 6.6 Lushan earthquake constrained by strong-motion and teleseismic data. *Seismological Research Letters, 85*(1), 15–22. https://doi.org/10.1785/0220130126.

Zhao, J. X., Zhang, J., Asano, A., Ohno, Y., Oouchi, T., Takahashi, T., et al. (2006). Attenuation relations of strong ground motion in Japan using site classification based on predominant period. *Bulletin of the Seismological Society of America, 96*(3), 898–913. https://doi.org/10.1785/0120050122.

(Received September 5, 2018, revised April 2, 2019, accepted April 3, 2019, Published online April 26, 2019)